Journal of Medical Imaging

MedicalImaging.SPIEDigitalLibrary.org

Improved reconstruction of phase-stepping data for Talbot–Lau x-ray imaging

Sebastian Kaeppler
Jens Rieger
Georg Pelzer
Florian Horn
Thilo Michel
Andreas Maier
Gisela Anton
Christian Riess

SPIE.

Sebastian Kaeppler, Jens Rieger, Georg Pelzer, Florian Horn, Thilo Michel, Andreas Maier, Gisela Anton, Christian Riess, "Improved reconstruction of phase-stepping data for Talbot–Lau x-ray imaging," *J. Med. Imag.* **4**(3), 034005 (2017), doi: 10.1117/1.JMI.4.3.034005.

Improved reconstruction of phase-stepping data for Talbot–Lau x-ray imaging

Sebastian Kaeppler,[a,*] Jens Rieger,[b] Georg Pelzer,[b] Florian Horn,[b] Thilo Michel,[b] Andreas Maier,[a] Gisela Anton,[b] and Christian Riess[a]
[a]Friedrich-Alexander-University Erlangen-Nuremberg, Pattern Recognition Lab, Department of Computer Science, Erlangen, Germany
[b]Friedrich-Alexander-University Erlangen-Nuremberg, Erlangen Centre for Astroparticle Physics, Department of Physics, Erlangen, Germany

Abstract. Grating-based Talbot–Lau x-ray interferometry is a popular method for measuring absorption, phase shift, and small-angle scattering. The standard acquisition method for this modality is phase stepping, where the Talbot pattern is reconstructed from multiple images acquired at different grating positions. We review the implicit assumptions in phase-stepping reconstruction, and find that the assumptions of perfectly known grating positions and homoscedastic noise variance are violated in some scenarios. Additionally, we investigate a recently reported estimation bias in the visibility and dark-field signal. To adapt the phase-stepping reconstruction to these findings, we propose three improvements to the reconstruction. These improvements are (a) to use prior knowledge to compute more accurate grating positions to reduce moiré artifacts, (b) to utilize noise variance information to reduce dark-field and phase noise in high-visibility acquisitions, and (c) to perform correction of an estimation bias in the interferometer visibility, leading to more quantitative dark-field imaging in acquisitions with a low signal-to-noise ratio. We demonstrate the benefit of our methods on simulated data, as well as on images acquired with a Talbot–Lau interferometer. [DOI: 10.1117/1.JMI.4.3.034005]

Keywords: Talbot–Lau; phase contrast; phase stepping; reconstruction; moiré.

Paper 17091RR received Apr. 7, 2017; accepted for publication Aug. 9, 2017; published online Sep. 5, 2017.

1 Introduction

Conventional x-ray imaging measures only the attenuation of x-rays. Recently, several measurement principles for phase sensitive x-ray imaging have been proposed. Most notable of these methods are propagation-based systems,[1] diffraction-enhanced systems,[2] edge-illumination,[3] and grating-based interferometers.[4,5] These systems represent different trade-offs between phase sensitivity, the ability to measure dark-field signals, setup complexity, and requirements on source coherence.

The clinical relevance of phase and dark-field signals has been extensively investigated, e.g., in Refs. 6–12. For example, phase and dark-field signals offer improved soft-tissue contrast in breast specimens compared to absorption x-ray alone.[13,14] Dark-field imaging has also shown potential for diagnosing lung diseases.[15,16] Among other phase sensitive systems, the grating-based Talbot–Lau interferometer is able to measure phase and dark-field signals. Additionally, it can be operated with a medical x-ray tube and detector. This makes this setup comparably well-suited for use in a medical environment.[17,18]

Figure 1 shows a sketch of a Talbot–Lau interferometer. The interferometer consists of a set of gratings, source grating G0, phase grating G1, and analyzer grating G2. At a design energy, the grating G1 imprints a periodic phase shift of either π or $\frac{\pi}{2}$ on the x-ray beam. When the G1 grating is illuminated with a coherent x-ray source, diffraction leads to the formation of an intensity self-image (also called Talbot pattern) at the Talbot distances downstream of G1. Since conventional x-ray sources typically do not fulfill the coherence requirements for the Talbot effect, the G0 grating is used to split the x-ray source into a set of slit sources that are coherent perpendicular to the grating bars. When the G0 parameters are matched to those of the G1 grating, Talbot imaging with conventional x-ray sources is possible.[5,19] The period of the G1 self-image is typically too small for direct detection with conventional x-ray detectors. To facilitate detection of the intensity pattern, the G2 grating is placed in front of the x-ray detector. The G2 period is chosen to match the period of the intensity pattern at the G2 position. The intensity at the detector then corresponds to the scalar product between the intensity pattern and the function describing the G2 grating bars. However, the intensity pattern cannot be directly characterized from one measurement alone. It has been proposed to detune the interferometer[20] or use a specially designed G2 grating[21] to create a spatial intensity modulation on the detector whose period is in the magnitude of the detector's pixel size. While these methods allow retrieving information about the Talbot pattern from a single image, they suffer from a loss of resolution due to the spatial information modulation, as well as a loss of visibility due to blurring in the detector's converter layer. Due to these limitations, the standard method of acquiring Talbot–Lau data is phase stepping, where multiple measurements are used to compute the information of the intensity pattern. During phase stepping, the G2 grating is translated by one G2 period perpendicular to the grating bars, while images are acquired at equidistant positions.

Since phase-stepping reconstruction is a key component of the Talbot–Lau imaging chain, any improvement to this step directly impacts the resulting image quality. In this paper, we review the implicit assumptions that are inherent in phase-stepping reconstruction and assess their validity. We find that two assumptions can be violated: the assumptions of perfectly

*Address all correspondence to: Sebastian Kaeppler, E-mail: sebastian.kaeppler@fau.de

2329-4302/2017/$25.00 © 2017 SPIE

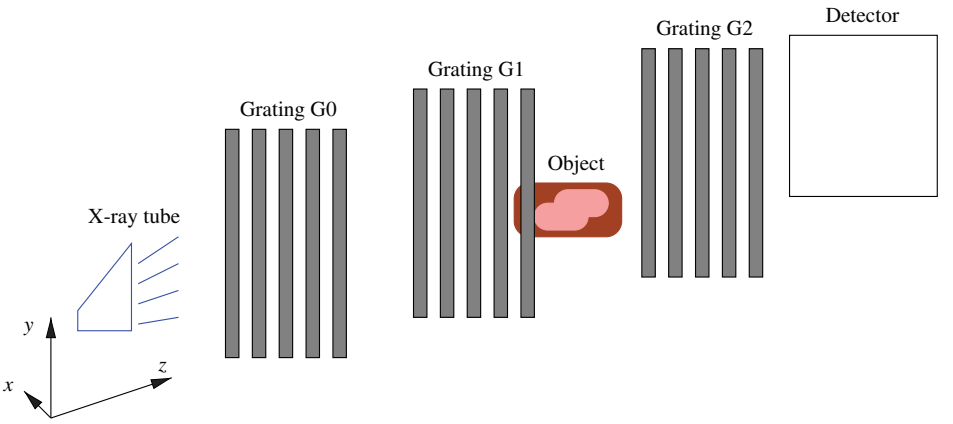

Fig. 1 Illustration of a Talbot–Lau interferometer. During phase-stepping acquisition, the grating G2 is translated in x-direction.

known phase-stepping positions and of equal noise variance in all measurements. We also investigate the origin of a recently reported estimation bias in dark-field images.[22] Based on this analysis, we propose three improvements to the phase-stepping reconstruction: an algorithm for estimating the true phase-stepping positions, a noise weighting to account for varying noise variances, and a visibility bias correction. Our proposed modifications are evaluated on real and simulated data.

The paper is organized as follows: In Sec. 1.1, we describe the standard phase-stepping reconstructing method. Afterward, we review the assumptions in phase-stepping reconstruction as well as the estimation bias and discuss prior work. In Sec. 2, we present our proposed improvements to the reconstruction, followed by experiments and discussion of each improvement in Sec. 3. We finish our paper with conclusions in Sec. 4.

1.1 *Phase-Stepping Reconstruction*

Typically, three types of information are obtained from the Talbot pattern: the mean intensity, the visibility (i.e., the contrast), and the phase. Thus, phase-stepping reconstruction requires a set of $N \geq 3$ measurements $\mathbf{m}_i = [m_i^1, \cdots, m_i^N]$ for each pixel $i \in [1; M]$. The superscript $j \in [1; N]$ denotes the corresponding phase-stepping positions $\mathbf{s} = [s^1, \cdots, s^N]$, $s^j \in [0; 2\pi[$. Under the assumption of a sinusoidal Talbot pattern, a sine function with three parameters (offset, amplitude, and phase) can be used to describe the pattern. The offset o corresponds to the mean intensity, the normalized amplitude (i.e., the amplitude divided by the offset), v, to the visibility, while the phase is denoted as p. This leads to the measurement model

$$m_i^j = o_i + o_i \cdot v_i \cdot \sin(p_i + s^j) + \eta_i^j, \tag{1}$$

for the i'th pixel. The term η_i^j corresponds to noise and deviations from the sinusoidal model. Figure 2 shows an idealized example of such a measurement, together with the fitted sine function.

To compute o_i, v_i, and p_i, the model is linearized using the trigonometric identity

$$\sin(p_i + s^j) = \sin(p_i) \cdot \cos(s^j) + \cos(p_i) \cdot \sin(s^j). \tag{2}$$

By substituting $c_i = o_i \cdot v_i \cdot \sin(p_i)$ and $d_i = o_i \cdot v_i \cdot \cos(p_i)$, Eq. (1) becomes

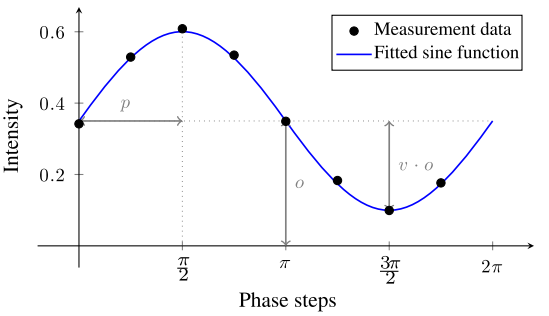

Fig. 2 Illustration of the phase-stepping reconstruction. The noisy measurement data are shown in black, while the fitted sine function is shown in blue.

$$m_i^j = o_i + c_i \cdot \cos(s^j) + d_i \cdot \sin(s^j) + \eta_i^j. \tag{3}$$

Since the phase-stepping positions $\mathbf{s}$ are assumed to be known from the acquisition process, o_i, c_i, and d_i can be retrieved by solving the linear least squares problem

$$\arg\min_{o_i, c_i, d_i} \sum_j \{m_i^j - [o_i + c_i \cdot \cos(s^j) + d_i \cdot \sin(s^j)]\}^2. \tag{4}$$

The least squares problem can be solved using standard methods. If the phase-stepping positions $\mathbf{s}$ lie equidistantly in the interval of $[0; 2\pi[$, the discrete Fourier transform can be used to directly obtain a solution for Eq. (4). In this case, o_i corresponds to the DC-component, and c_i and d_i correspond to the real and imaginary parts of the lowest frequency component, respectively. Afterward, the visibility v_i and phase p_i can be computed as

$$v_i = \frac{\sqrt{(c_i)^2 + (d_i)^2}}{o_i} \tag{5}$$

and

$$p_i = \tan^{-1} \frac{c_i}{d_i}. \tag{6}$$

In Talbot–Lau imaging, inhomogeneities of the gratings and imperfect grating positioning require the acquisition of two images, a reference image without the object in the beam

path and an object image with the object. We subsequently denote the offset, visibility, and phase corresponding to the reference image pixels as o_i^{r}, v_i^{r}, and p_i^{r}, and those belonging to the object image pixels as o_i^{o}, v_i^{o}, and p_i^{o}. The object attenuation a_i is then computed as the log-ratio of the mean intensities

$$a_i = -\log\left(\frac{o_i^{\mathrm{o}}}{o_i^{\mathrm{r}}}\right), \tag{7}$$

the differential phase h_i as

$$h_i = p_i^{\mathrm{o}} - p_i^{\mathrm{r}}, \tag{8}$$

and the dark-field signal f_i as

$$f_i = 1 - \frac{v_i^{\mathrm{o}}}{v_i^{\mathrm{r}}}. \tag{9}$$

1.2 *Assumptions Used in Phase-Stepping Reconstruction*

The reconstruction of phase-stepping data is based on a set of underlying assumptions on the measured data. In this section, we describe and review the validity of these assumptions.

1.2.1 *Sinusoidal interference pattern*

Phase-stepping reconstruction seeks to reconstruct a sinusoidal signal. In contrast, an ideal monochromatic Talbot–Lau system with an x-ray point source produces a triangular intensity pattern after the G2 grating. This triangular pattern can be interpreted as a superimposition of sinusoidal patterns with different frequencies. However, the blurring of the Talbot pattern due to the size of the actual x-ray source or due to the width of the G0 slits leads to an attenuation of the high-frequency components of the triangular pattern, such that it can be approximated by a single sine function. This sinusoidal approximation is valid for typically used G0 slit sizes.[19]

1.2.2 *Data consistency during phase stepping*

It is assumed that the object does not change during the acquisition of the phase-stepping curve. Similar to conventional x-ray imaging, movement of the object in the order of magnitude comparable to the pixel size during acquisition introduces motion artifacts. In Talbot–Lau interferometry, movement may lead to inconsistency in the phase-stepping curve and hence introduce artifacts. This can be avoided by properly fixating the scanned sample, proper animal sedation, or patient instruction. In addition, acquisition parameters, such as exposure time, tube voltage, and tube current, need to be kept constant during the acquisition process. This, however, is typically not a problem when using modern x-ray tubes. However, high-frequency oscillations of the gratings during the acquisition of a phase step may reduce the visibility of the interferometer for individual phase steps and lead to inconsistent phase-stepping data.

1.2.3 *Error-free phase-stepping positions*

Phase-stepping reconstruction requires knowledge about the phase-stepping position of each measurement. The actual phase stepping is typically performed by translating the G2 grating using a piezoelectric motor, such that the positions of the G2 grating can be obtained from the motor programming. However, in practice, vibrations or motion affecting the setup during the phase-stepping acquisition may lead to uncontrolled translation of the G2 grating versus the G1 and thus to a change in the actual phase-stepping position. These vibrations are typically due to external influences, e.g., building vibrations, which transfer to the gratings. This makes estimating their distribution and typical magnitude very difficult. A translation t of the G2 grating perpendicular to the grating bars leads to shift of phase-stepping position

$$\Delta s = \frac{2\pi t}{p_2}, \tag{10}$$

where p_2 is the period of the G2 grating. Since the period is typically in the range of a few micrometers, stability of the setup at nanometer scale is required during the phase-stepping acquisition. This stability is particularly difficult to achieve without the use of a stabilized optical table and is an issue that needs to be addressed in both experimental and (pre) clinical systems. Figure 3 shows a dark-field and a differential phase image acquired with a Talbot–Lau system that was mounted vertically to mimic a clinical mammography system. The sample is superimposed by moiré patterns. This is due to the fact that the phase step images typically exhibit moiré patterns in Talbot–Lau imaging. Deviations from of the actual phase-stepping positions in either the reference or the object phase-stepping acquisition lead to an incorrect combination of the information contained in the phase-step images and thus to the formation of moiré artifacts in the reconstructed images.

1.2.4 *Equal noise variance in each measurement*

The phase-stepping reconstruction does not make any assumptions about noise in the measured data. The linear least squares method used for reconstruction is a maximum-likelihood estimator under the assumption of a zero-mean Gaussian distribution of the noise term η_i^j, with equal variance for each phase step. Using modern flat-panel x-ray detectors, two types of noise dominate η_i^j: Poisson distributed quantum noise and electronic noise, which is typically modeled as a zero-mean Gaussian with a detector-dependent variance. While the distributions of the electronic noise match the assumptions of the phase-stepping reconstruction, the distributions of the quantum noise do not. Since each measurement m_i^j is located at a different position of the sinusoidal phase-stepping curve, the measurements on top of the curve result from more photons than the measurements on the bottom of the curve. Since the variance of the Poisson distribution is equal to the number of photons, the assumption of equal noise variance in each measurement is violated. The degree of the deviation of the true noise statistics from the noise model used in reconstruction is dependent on the visibility v_i, where a higher visibility corresponds to a stronger deviation.

1.2.5 *Unbiased estimates*

Unbiasedness is an important property of a statistical estimator. It means that there is no difference between the expected value of the estimator and the true value of the quantity that is being estimated (i.e., there is no systematic difference between the true value and the estimator output). This is a critical issue when performing quantitative imaging. Marschner et al.[22] have recently

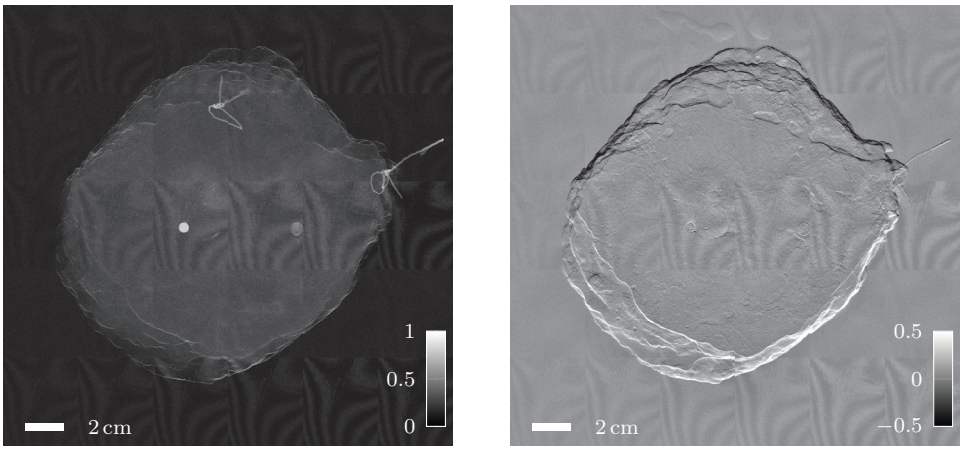

Fig. 3 Images of a human breast mastectomy specimen, acquired with a Talbot–Lau interferometer by tiling smaller images: (a) dark-field and (b) differential phase. Some image tiles are affected by moiré artifacts.

shown that the phase-stepping reconstruction exhibits a bias for the visibility and dark-field information. Specifically, this bias corresponds to an overestimation of the visibility. The magnitude of the bias is inversely related to the visibility signal-to-noise (SNR) ratio.

1.3 *Prior Work*

Few methods have been proposed to improve the standard approach for reconstruction of phase-stepping data. Modregger et al.[23] proposed a deconvolution-based approach for information retrieval, which does not depend on the assumption of a sinusoidal phase-stepping curve. The noise properties of this algorithm were later investigated by Weber et al.[24] Yang et al.[25] developed a phase-stepping reconstruction method for nonideal gratings, which may exhibit a phase-stepping curve with twin peaks. The problem of estimating the position of misaligned phase steps was considered by Pelzer et al.[26] and Seifert et al.[27] They showed that an algorithm known in optics[28] can be used to retrieve the correct phase-stepping positions, if the Talbot–Lau interferometer is detuned by rotation of either G1 or G2, such that sufficient moiré fringes appear in the reference phase, and if a sufficient number of phase steps are available. However, detuning the interferometer reduces visibility. Marschner et al.[29] proposed a method based on expectation maximization that seeks to locally adjust the phase-stepping positions such that the measurement model is most consistent with the measurements. This approach relies on the assumption that the measurement data are consistent and that the deviations of the positions are not strong. The use of noise variance information to account for quantum noise has been mentioned in literature, e.g., in Refs. 30, but there exists—to our knowledge—no full derivation or systematic evaluation of this approach. Also, these approaches do not model the detector read-out noise. Two approaches have been proposed to retrieve information from less than three phase steps. Marschner et al.[22] proposed a method for retrieving dark-field information from only two phase steps. While this method does not exhibit a bias for the visibility and dark-field information, it relies on the assumption of zero phase shift, as phase information cannot be recovered using this method. Pelliccia et al.[31] proposed a reconstruction method based on Taylor expansion for three phase steps. Their method can be extended to allow reconstruction of phase information from two phase steps, under the assumption of a negligible dark-field signal.

2 Methods

We propose a set of improvements for the phase-stepping reconstruction method. Our modifications seek to solve problems that arise from violations common in phase-stepping reconstruction. Our contribution consists of three improvements:

- A method for estimation of the true phase-stepping positions. This approach is based on two steps: an optional preprocessing step that identifies and discards inconsistent phase-stepping data, followed by an optimization-based estimation of the true phase-stepping positions that seeks to maximize the spatial homogeneity in the reconstructed image.
- A modification of the least squares reconstruction to take varying noise variances due to both quantum and detector read-out noise into account.
- The application of a bias correction to the estimated visibility to correct systematic estimation errors in the visibility and dark-field images.

Each method and the changes to the standard phase-stepping reconstruction are independent of each other. The methods are described in the following sections.

2.1 *Phase-Stepping Position Correction*

Several algorithms to recover unknown phase-stepping positions are known in the field of optics. However, these algorithms typically use assumptions about the reconstructed signal that cannot always be fulfilled in Talbot–Lau imaging: low attenuation, uniform distribution of the phases $\mathbf{p}$, uniform distribution of the stepping positions $\mathbf{s}$, consistent measurement data, and/or a certain number of phase steps. For example, the method used by Pelzer et al.[26] and Seifert et al.[27] assumes uniformly

distributed phases and low attenuation, while the method by Marschner et al.[29] assumes consistent measurement data and requires at least four phase steps.

Our goal is to develop an alignment algorithm that is not based on these assumptions. The proposed algorithm consists of two steps: first, discarding heavily misaligned or inconsistent phase steps. Second, local realignment of the remaining phase steps by minimizing the variations in the reconstructed offsets and visibilities.

2.1.1 *Discarding inconsistent phase steps*

In a first optional preprocessing step, we seek to discard heavily misaligned phase steps, which are inconsistent with the majority of the other phase steps. This step is beneficial if the error in phase-stepping position is large, as the subsequent realignment works only locally. To detect misaligned phase steps, we calculate a consistency criterion for each phase step image. We first perform the standard phase-stepping reconstruction as described in Sec. 1.1 using the assumed positions of the G2 grating. Afterward, we calculate the squared consistency error e_i^j for each measurement pixel m_i^j

$$e_i^j = \{m_i^j - [o_i + c_i \cdot \cos(s^j) + d_i \cdot \sin(s^j)]\}^2. \tag{11}$$

This error corresponds to the squared fitting error of Eq. (4). The error is averaged over the whole image, i.e.,

$$e^j = \frac{1}{M}\sum_i e_i^j. \tag{12}$$

Assuming no model error and accurate phase-stepping positions, the only source of the error in e^j is noise. Due to the averaging over all image pixels, the amount of noise should be approximately equal for each phase step. However, deviations from the correct phase-stepping positions lead to an increased error. Thus, we seek to identify inconsistent phase steps, by noting that their error is much larger than the average error of all phase steps. To this end, we use median absolute deviation[32] to estimate the standard deviation $\hat{\sigma}_e$ of the errors of the phase steps

$$\hat{\sigma}_e = 1.4826 \cdot \text{median}[|\mathbf{e} - \text{median}(\mathbf{e})|], \tag{13}$$

where $\mathbf{e} = [e^1, \cdots, e^j]$ is the vector of fitting errors for each phase-stepping image. Compared to the standard method of estimating the standard deviation, the median absolute deviation is more robust in the presence of outliers. We then discard all phase steps whose corresponding error e^j exceeds a predetermined threshold $\tau \cdot \hat{\sigma}_e + \text{median}(\mathbf{e})$. The parameter τ should be chosen large enough, such that only those phase steps are discarded that cannot be corrected by the subsequent realignment procedure.

2.1.2 *Estimation of the phase-stepping positions*

After discarding inconsistent phase-stepping data, we seek to compute the true phase-stepping positions, using the assumed stepping positions as a starting point. This estimation is based on prior knowledge about the relationships of the offset, visibility, and phase information. Recall that in phase-stepping reconstruction, we solve the least squares problem

$$\arg\min_{o_i,c_i,d_i} \sum_j \{m_i^j - [o_i + c_i \cdot \cos(s^j) + d_i \cdot \sin(s^j)]\}^2. \tag{14}$$

Since the above equation is a linear least squares problem, its solution is given by

$$o_i = \sum_j w_o^j \cdot m_i^j, \quad c_i = \sum_j w_c^j \cdot m_i^j, \quad d_i = \sum_j w_d^j \cdot m_i^j, \tag{15}$$

where $\mathbf{w_o} = [w_o^1, \cdots, w_o^N]$, $\mathbf{w_c} = [w_c^1, \cdots, w_c^N]$, and $\mathbf{w_d} = [w_d^1, \cdots, w_d^N]$ are a set of weights that can be obtained from inversion of the measurement matrix containing the phase-stepping positions $\mathbf{s}$. Since o_i has to correspond to the offset of the sine function, while c_i and d_i must not contain the offset, we have

$$\sum_j w_o^j = 1, \quad \sum_j w_c^j = 0, \quad \sum_j w_d^j = 0. \tag{16}$$

In the case where the phase-stepping positions are misaligned, the weights are incorrectly determined. For example, a misaligned phase step at position k results in the weights w_o^k, w_c^k, and w_d^k being either too large or too small compared to the other weights, i.e., too much or too little of the phase step image $\mathbf{m}^k$ gets added to the images $\mathbf{o}$, $\mathbf{c}$, and $\mathbf{d}$. As a consequence, $\mathbf{o}$, $\mathbf{c}$, and $\mathbf{d}$ are either over- or underestimated. However, due to the constraints in Eq. (16), only the phase modulation $\mathbf{o} \cdot \mathbf{v} \cdot \sin(\mathbf{p} + s^k)$ of the Talbot pattern, but not its offset, contributes to the estimation error.

The phase modulation in Talbot–Lau imaging typically shows moiré fringes. Since the estimation error is then propagated through the formulas for computing the attenuation, differential phase, and dark-field images, the resulting image artifacts resemble the moiré structure of the phase modulation, transformed by the reconstruction function.

Our approach for estimating the phase-stepping positions is based on the assumption that the phase modulation of the Talbot–Lau interferometer is not correlated with the offset and visibility images $\mathbf{o}$ and $\mathbf{v}$, which we seek to reconstruct. This assumption is justified, as the phase modulation is dominated by the reference phase, which depends mostly on the gratings positions. If the phase-stepping positions are incorrect, the phase modulation is transferred into the reconstructed images. Under that assumption of noncorrelated signals, this increases the variance in $\mathbf{o}$ and $\mathbf{v}$. Thus, to find the correct phase-stepping positions, we must try to minimize with respect to the phase-stepping positions some measure of variance in the offset and the visibility images.

A degenerate solution for the phase-stepping positions may lead to a drop in visibility, and thus also in a drop in its variation. We normalize visibility and offset to avoid this issue. Let $\mathbf{v}(\mathbf{s}^*)$ and $\mathbf{o}(\mathbf{s}^*)$ be the visibility and offset images reconstructed with phase-stepping positions $\mathbf{s}^*$ using the standard method described in Sec. 1.1, respectively. We define the normalized visibility $\mathbf{v}'(\mathbf{s}^*)$ and normalized offsets $\mathbf{o}'(\mathbf{s}^*)$ as

$$\mathbf{v}'(\mathbf{s}^*) = \frac{\mathbf{v}(\mathbf{s}^*)}{\frac{1}{M}\sum_i v_i(\mathbf{s}^*)} \tag{17}$$

and

$$\mathbf{o}'(\mathbf{s}^*) = \frac{\mathbf{o}(\mathbf{s}^*)}{\frac{1}{M}\sum_i o_i(\mathbf{s}^*)}. \tag{18}$$

We then seek to minimize the following optimization problem to obtain the new set of phase-stepping positions $\mathbf{s}'$

$$\mathbf{s}' = \arg\min_{\mathbf{s}^*} \|\nabla[\mathbf{g} * \mathbf{v}'(\mathbf{s}^*)]\|_1 + \|\nabla[\mathbf{g} * \mathbf{o}'(\mathbf{s}^*)]\|_1. \tag{19}$$

Here, $\|\nabla.\|_1$ denotes the $L1$-norm of the image gradient, i.e., the total variation of the image, while $\mathbf{g}$ corresponds to a Gaussian filter with standard deviation σ_g that we convolve with the reconstructed images to remove noise. Optimization of this function is challenging. The computation of $\mathbf{v}(\mathbf{s}^*)$ and $\mathbf{o}(\mathbf{s}^*)$ itself requires solving a least squares problem. The corresponding measurement model is based on the phase-stepping positions after transformation by a trigonometric function [see Eq. (3)]. As these trigonometric functions, as well as the normalization function for offset and visibility, are nonconvex, the optimization problem in Eq. (19) is also nonconvex. Thus, convergence to a global optimum cannot be guaranteed. However, in practice, the nonconvexity is not an issue for determining accurate stepping positions when heavily misaligned phase steps are removed using the proposed preprocessing method.

For optimization, we utilize the Broyden–Fletcher–Goldfarb–Shanno method[33] and use the assumed phase-stepping position as an initial solution. Analytic computation of the gradients is difficult for more than three phase steps due to the matrix inversion required for solving the inner least squares problem. Thus, we compute the gradients using finite differences. After determining the updated phase-stepping positions $\mathbf{s}'$, the normal phase-stepping reconstruction can be carried out using the new set of stepping positions.

2.2 *Noise Variance Weighting*

In this step, we seek to incorporate noise variance information into the phase-stepping reconstruction. The standard method for phase-stepping reconstruction is solving the least squares problem

$$\arg\min_{o_i,c_i,d_i} \sum_j \{m_i^j - [o_i + c_i \cdot \cos(s^j) + d_i \cdot \sin(s^j)]\}^2. \tag{20}$$

As discussed in Sec. 1.2, this step yields a maximum-likelihood estimate when there is noise of equal variance in each measurement m_i^j. However, in reality, quantum noise is Poisson distributed. If an energy-integrating detector is used, electronic noise also contributes to the noise in the measurement. As electronic noise is often modeled as a zero-mean Gaussian, the noise in m_i^j is in fact the sum of Poisson and Gaussian noise. As this effect is not modeled in the reconstruction process, the reconstructed data may show more noise than necessary. We seek to modify the measurement model to account for the noise statistics to alleviate this problem. We approximate the sum of the two noise distributions by a Gaussian distribution, i.e., we approximate the Poisson distribution using only its variance. The assumed variance of the measurement, $(\hat{\sigma}_i^j)^2$, is thus the variance of the electronic noise, $(\sigma_e)^2$, plus the variance of the quantum noise. The electronic noise variance can be obtained by calibration. The variance of the quantum noise can be approximated by a Poisson distribution with an expected value of the measurement value m_i^j. Note that for an energy-integrating detector, when electronic noise is assumed, it may be necessary to apply a correction factor to m_i^j that relates the arbitrary units recorded by the detector to the detected number of photons to obtain proper scaling between quantum and electronic noise. The estimated noise variance $(\hat{\sigma}_i^j)^2$ depends on both pixel- and phase-stepping position and is computed as

$$(\hat{\sigma}_i^j)^2 = m_i^j + (\sigma_e)^2. \tag{21}$$

The expected noise variance can then be included in the objective function, yielding

$$\arg\min_{o_i,c_i,d_i} \sum_j \frac{1}{(\hat{\sigma}_i^j)^2} \cdot \{m_i^j - [o_i + c_i \cdot \cos(s^j) + d_i \cdot \sin(s^j)]\}^2. \tag{22}$$

The resulting optimization problem is now a weighted least squares problem but can still be solved by matrix inversion. At least four phase steps are required to obtain a different result compared to the standard method, since more measurements than unknowns are required to allow for data weighting. The measurement matrix of the weighted least squares problem now depends on the pixel position i, i.e., one matrix inversion is required for each pixel, instead of only one inversion for all pixels. After solving the least squares problems, the remaining steps of the phase-stepping reconstruction can be performed identically to the standard approach.

2.3 *Visibility Bias Correction*

In this step, we seek to correct systematic overestimation of visibility information. In phase-stepping reconstruction, the visibility is computed as

$$v_i = \frac{\sqrt{(c_i)^2 + (d_i)^2}}{o_i}. \tag{23}$$

This corresponds to the magnitude of c_i and d_i, divided by the offset o_i. Marschner et al.[22] observed that this estimation step exhibits a bias when approaching a low SNR, i.e., the visibility is systematically overestimated. However, they proposed no correction method that can be applied within the standard phase-stepping reconstruction. The fact that magnitude computations of noisy data of the form $\sqrt{(x^2)}$ exhibit an overestimation bias is well-known in MR imaging.[34] For the case of $\sqrt{(x^2)}$, where x is a complex number, the expected value of the estimator is not $|x|$, but rather $\sqrt{x^2 + \sigma_x^2}$, where σ_x^2 is the noise variance in the real and imaginary part of x. In the case of Talbot–Lau imaging, this leads to the situation where v_i is overestimated by the bias b_i

$$b_i = \frac{\sqrt{(c_i)^2 + (d_i)^2 + (\sigma_i^{cd})^2} - \sqrt{(c_i)^2 + (d_i)^2}}{o_i}. \tag{24}$$

Here, $(\sigma_i^{cd})^2$ corresponds to the noise variances of c_i and d_i. Under a quantum noise model, Weber et al.[35] have shown that $(\sigma_i^{cd})^2$ is two times the true offset that generated the measurement data (if we consider electronic noise, plus two times the variance of the electronic noise), divided by the number of phase steps N. The true offset can be approximated by the

reconstructed offset o_i. We can thus calculate the approximate noise variance $(\hat{\sigma}_i^{cd})^2$ as

$$(\hat{\sigma}_i^{cd})^2 = \frac{2 \cdot [o_i + (\sigma_e)^2]}{N}. \tag{25}$$

Gudbjartsson and Patz[34] proposed the corrected magnitude estimator $\sqrt{x^2 - \sigma_x^2}$ to correct for the estimation bias. We apply this estimator to the visibility and calculate the bias-corrected visibility v_i' as

$$v_i' = \begin{cases} \frac{\sqrt{(c_i)^2 + (d_i)^2 - (\hat{\sigma}_i^{cd})^2}}{o_i}, & \text{if } (c_i)^2 + (d_i)^2 - (\hat{\sigma}_i^{cd})^2 > 0 \\ 0 & \text{otherwise} \end{cases}. \tag{26}$$

Subsequent computation of the dark-field image is performed as with the standard algorithm.

3 Experiments and Discussion

In this section, we describe the experiments used to evaluate the proposed improvements to the phase-stepping reconstruction. Experiments are performed on both simulated and real data. We evaluate each proposed modification independently from the other ones.

3.1 *Acquisition of Talbot–Lau X-Ray Images*

Real data were acquired with a three-grating Talbot–Lau interferometer. The grating size was 24.14 mm × 13.27 mm, the periods were 24.39 μm (G0), 3.37 μm, and 2.4 μm for G1 and G2, with a G1–G2 distance of 159 mm. The design energy of the system was 25 keV, while the x-ray tube was operated at a peak voltage of 40 kVp at 60-mA current. The number of phase steps was between 5 and 21. Additional details of the setup can be found in Ref. 36. The images show cancerous human mastectomy samples. The data were acquired within a study that has been approved by the ethics committee of the University Hospital Erlangen in the medical faculty of the Friedrich-Alexander-University Erlangen-Nuremberg. Written informed consent has been obtained from the patients. Due to the large size of the objects, the final images were stitched from 20 to 90 tiles. The setup was arranged vertically to imitate a typical mammography system. Due to the lack of vibration dampening, phase drift artifacts and moiré artifacts affected the image quality in some data sets. To reduce low-frequency phase drift artifacts, we applied a correction algorithm[37] before stitching the image tiles.

3.2 *Phase-Stepping Position Correction*

We pursued two types of experiments for the proposed phase-stepping position estimation: (a) a quantitative evaluation on simulated data with controlled variations of the true phase-stepping positions, where we had access to ground truth information and (b) an evaluation on data acquired with a Talbot–Lau interferometer. We assess the image quality of the acquired data both quantitatively by measuring the image variation in a homogenous area, as well as qualitatively by visual inspection. In each experiment, we compare the standard phase-stepping reconstruction with the reconstruction using the phase-stepping positions provided by our method. We selected the parameters of our method based on a pilot experiment. The parameters were thresholding parameter $\tau = 10$ and Gaussian standard deviation $\sigma_g = 1$.

3.2.1 *Evaluation using simulated data*

We created attenuation and phase-shift projection images of the XCAT phantom[38] using the CONRAD framework.[39] The images had a size of 512 × 512 pixels. The phase-shift projection was differentiated and scaled to mimic a typical differential phase image obtained with a Talbot–Lau interferometer. Since no complete analytical model of the dark-field signal is known, the attenuation and differential phase image were used to define visibility loss due to beam hardening and unresolved edges. The reference phase was defined by a radial function around the image center. The corresponding images are shown in Fig. 4. The reference photon count and visibility were homogeneous over the whole image. The reference photon count was 1000 photons per phase step, and the visibility was 30%. Seven phase steps, uniformly distributed in the interval $[0; 2\pi[$, were generated with quantum noise for both reference and object images.

The true distribution of the phase-stepping error is difficult to obtain, due to its origin from random vibrations. We, therefore, conducted two experiments to investigate the performance of our algorithm for error distributions of different types and widths. For each experiment, we reconstructed the attenuation, dark-field, and differential phase images with the standard method and with the proposed phase-stepping position correction. Afterward, we calculated the root-mean-squared error (RMSE) between the reconstructed images and the ground truth images. Each experiment was repeated 200 times to obtain both mean and standard deviation for the RMSE. In the first experiment, we added zero-mean Gaussian noise to the phase-stepping positions of both reference and object image. The standard deviation of the noise was varied between 0.0 and 1.0 with an interval of 0.2. For the second experiment,

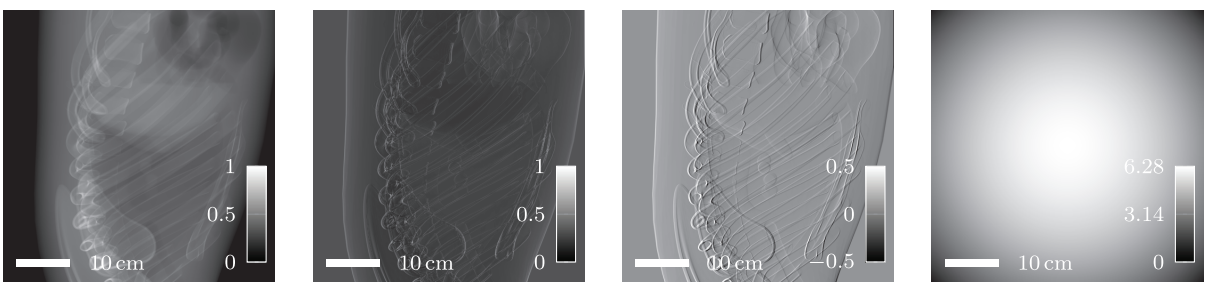

Fig. 4 Simulated images used for evaluation of the phase-stepping alignment: (a) attenuation, (b) dark-field, (c) differential phase, and (d) reference phase.

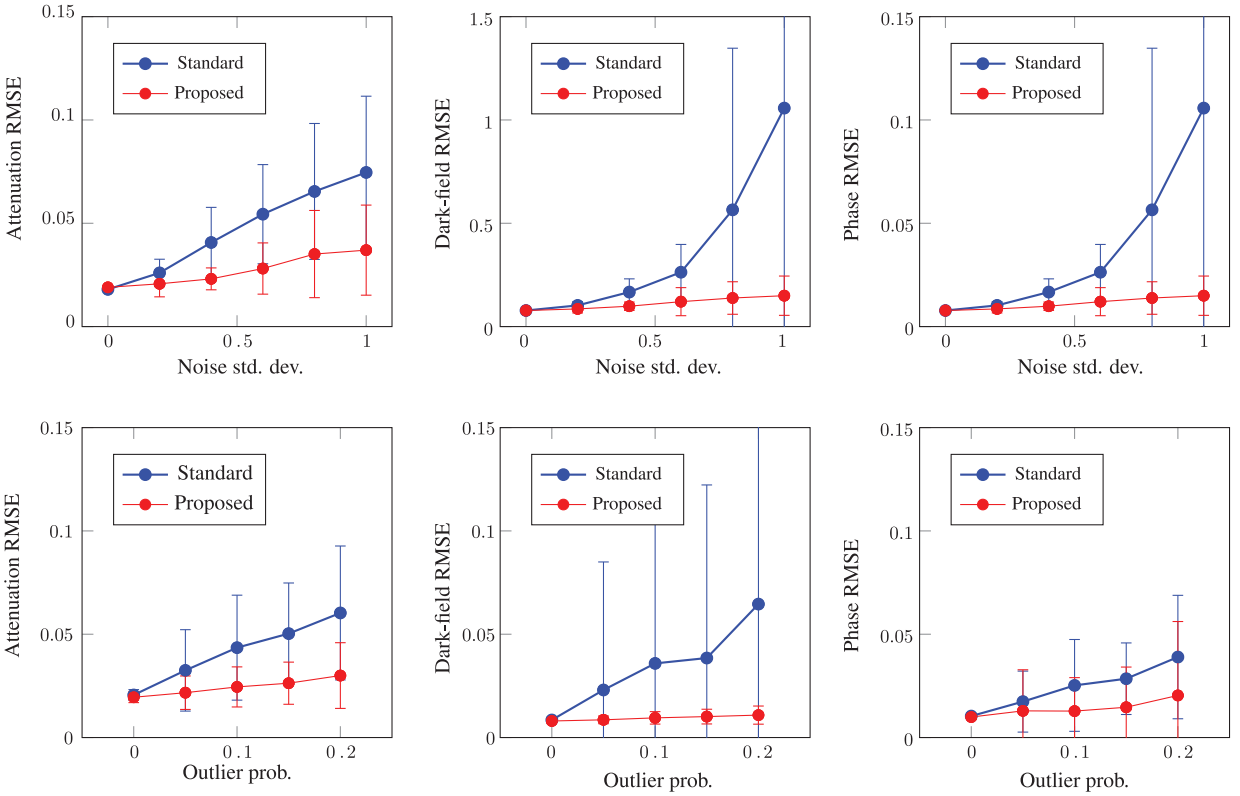

Fig. 5 Quantitative evaluation of the phase-stepping position estimation on simulated data. Each plot shows mean and standard deviation of the RMSE to the ground truth averaged over the whole image. In the experiment in the top row, Gaussian noise of varying magnitude was added to the phase-stepping positions. In the experiment shown in the bottom row, we varied the probability of observing an outlier phase step. An outlier phase step is assigned a random position drawn from an uniform distribution. Additionally, Gaussian noise of standard deviation 0.1 was added to all stepping positions. Compared to the standard method, the proposed algorithm reduces artifacts from misaligned phase steps.

we added zero-mean Gaussian noise with a standard deviation of 0.1 to all phase-stepping positions. Additionally, we defined an outlier probability. The outlier probability defines the probability for assigning a random position in the interval $[0; 2\pi[$ to a phase step. In the second experiment, we vary this outlier probability between 0 and 0.2 with an interval of 0.05.

The results of the experiments are shown in Fig. 5. The results for varying the standard deviation are shown in the top row, while the results for varying the outlier probability are shown in the bottom row. When no noise is added to the phase-stepping positions, the RMSE is dominated by quantum noise. For the standard method, slight deviation of the phase-stepping position leads to strong increase in the RMSE of dark-field and differential phase images. On an absolute scale, the effect on the attenuation image was weaker than on dark field and phase. In all experiments, the mean RMSE of attenuation, phase, and dark field produced by our method is below the mean RMSE of the standard method when the phase-stepping positions contain noise. The improvement provided by our method grows with increasing noise on the stepping positions. In the case where no noise was added to the stepping positions, our algorithm leads to a marginal increase in error for the attenuation image but not for the differential phase and dark-field images. The additional runtime for adjusting the phase-stepping positions was 3.8 ± 0.5 s per image on a standard laptop (DELL M4800, Intel Core i7-4910MQ CPU, 32 GB RAM, MATLAB® 2014b).

3.2.2 *Evaluation using real data*

We selected 11 of the breast data sets that were captured with our Talbot–Lau interferometer. We used the breast data instead of a dedicated phantom to assess the performance of the proposed algorithm within a realistic imaging protocol both quantitatively (outside of the specimen) as well as qualitatively (inside of the specimen). All data sets showed moiré artifacts in the attenuation, dark-field, or phase image. For all images from the standard reconstruction, we manually annotated a homogeneous area outside of the breast specimen that contained moiré artifacts. The only objects in the annotated areas are two polymethyl methacrylate (PMMA) slabs that are used to fix the breast specimen. Hence, we would expect constant absorption and dark-field, as well as zero differential phase shift in these regions. In practice, image noise, stitching artifacts at tile edges and variations due to long-term drifts of the phase, and moiré artifact can be visible. Removing or reducing the moiré artifacts can be expected to increase the homogeneity in the annotated region. To quantify the homogeneity, we computed the standard deviation of attenuation, dark-field, and differential phase in this area. The area was chosen such that it contained at least 10,000 pixels to ensure reliable estimation of the standard deviation. Afterward, we divided the standard deviation of the proposed method by the standard deviation of the standard method. Due to this normalization, a number lower than 1 corresponds to improved homogeneity in the

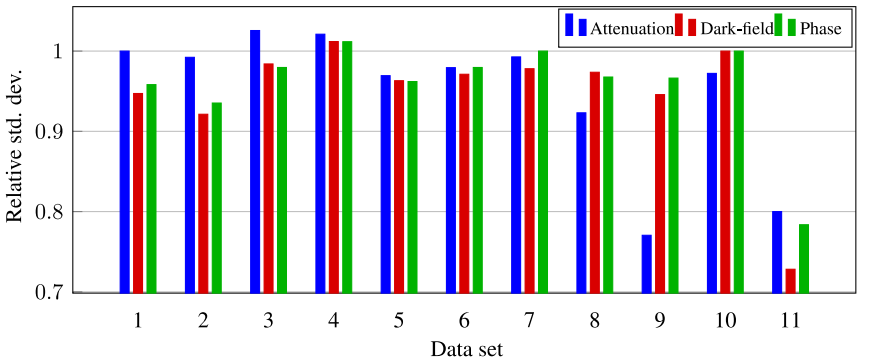

Fig. 6 Quantitative evaluation of the phase-stepping position realignment on data acquired with a Talbot–Lau interferometer. The bars show the standard deviation in a homogenous image region, reconstructed with the estimated phase-stepping positions, divided by the standard deviation in the same region, and reconstructed with the standard phase-stepping reconstruction. The proposed method leads to a lower standard deviation for all data sets, but number three and four.

marked region. The results are shown in Fig. 6. The proposed method achieved a better homogeneity for all images, except for the attenuation image of data set 3 and the images of data set 4, where the homogeneity is slightly decreased.

Afterward, we visually inspected all images. First, we investigated whether the proposed algorithm introduced new artifacts into the images or led to an increase of existing moiré artifacts. This was not the case for any of the images. The proposed algorithm managed to remove most moiré artifacts. In some cases of severe moiré, the moiré was only reduced but not removed. Figure 7 shows such a severe case. The amount of moiré removal was not always reflected in the reduction in standard deviation. We hypothesize that this is due to the fact that moiré artifacts correspond to slight low-frequency variations, which are difficult to quantify, while the image standard deviation is dominated by image noise. As our method can discard phase steps in cases of severe misalignment, it may have slightly increased the image noise when reducing moiré artifacts.

To further investigate this finding, we computed the noise power spectrum (NPS) for a homogenous 200×200 pixel region of data set 4, where our method had a higher standard deviation than the standard method. We applied radial averaging to obtain the radial NPS and divided the NPS of the proposed method by the NPS of the standard method to obtain a relative measure. The results are shown in Fig. 8. For low frequencies, the radial NPS of our method is an order of magnitude lower than the NPS of the standard method. For higher frequencies, the NPS of the proposed method is indeed slightly higher, contributing to the higher standard deviation.

3.2.3 *Discussion*

The experimental results on both simulated as well as on acquired data show that the proposed method is effective in reducing moiré artifacts arising from misaligned phase steps. Due to the presence of noise, other artifacts, and the varying amount of moiré, it is difficult to provide quantitative comparisons on real data. This is reflected by the varying degree of reduction in standard deviation in the homogenous region of interest across data sets. However, the frequency-dependent analysis using the NPS, where our method reduced low-frequency components, is consistent with the visual impression of the resulting images. While our method was able to almost completely remove moiré artifacts in acquired data, some residual artifacts remained in the case of severe moiré. We attribute this to the fact that the optimization problem used to align the phase steps is nonconvex and thus may not yield a globally optimal solution when phase steps are heavily misaligned. We used the same algorithmic parameters for synthetic and real data. Tuning these parameters to the amount of noise and position misalignment may improve results but is out of the scope of this work. For future work, it may also be interesting to replace the phase-stepping removal step of our method with a method that seeks to prealign heavily misaligned phase steps via exhaustive search.

In the experiment with simulated data, we measured a slight reduction in image quality of the attenuation image when the phase steps are perfectly aligned with their true positions. This finding could not be confirmed with the acquired data, where visual image quality always improved. We hypothesize that this is because data acquired with a real Talbot–Lau interferometer always have slight deviations in the phase-stepping positions. We conclude that the proposed method improves image quality by reducing moiré in cases where absolute stability of the interferometer cannot be guaranteed.

3.3 *Noise Variance Weighting*

Evaluation of the noise variance weighting was carried out using Monte Carlo simulation. We generated phase-stepping data affected by quantum noise. Afterward, we reconstructed offset, visibility, and phase using the standard method and using the proposed noise weighting. Then, we computed the RMSE of the reconstructed values to the ground truth data. Afterward, we divided the RMSE obtained with noise weighting by the RMSE of the standard approach to obtain a relative measure for noise. We evaluated 100,000 noise realizations for each data point, such that the standard deviation of the relative RMSE became negligible. Our baseline scenario is a phase-stepping curve with an offset corresponding to 1000 photons, a visibility of 0.5, a random phase, and 7 phase steps. First, we vary the number of phase steps between 3 and 11. In a second experiment, we vary the visibility between 0.1 and 0.7 with an interval of 0.1. In a third experiment, we vary the offset between 200 and 1000 photon counts in an interval of 100 counts. Figure 9 shows the results of the experiments. The results show that the benefit of the noise weighting is independent of the number of phase steps, as long as the number of phase steps exceeds three. In contrast to visibility and phase,

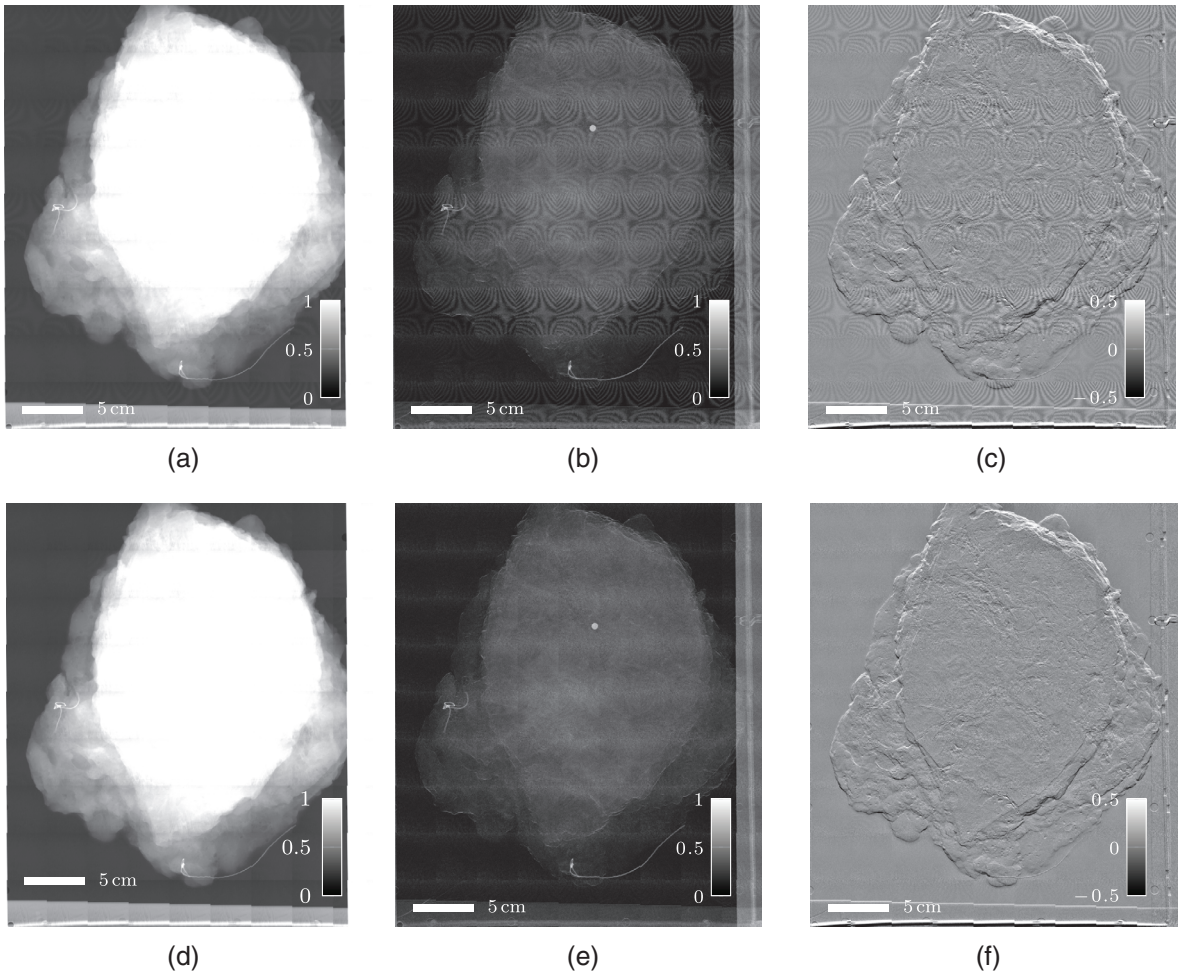

Fig. 7 A sample image showing severe moiré artifacts (data set 3). Top row: standard method and bottom row: proposed algorithm. (a and d) Attenuation, (b and e) dark-field, and (c and f) differential phase. The windowing in the attenuation image has been selected to reveal slight moirés in the bottom of the image. The images reconstructed with the proposed phase-stepping realignment method shows almost no moiré artifacts.

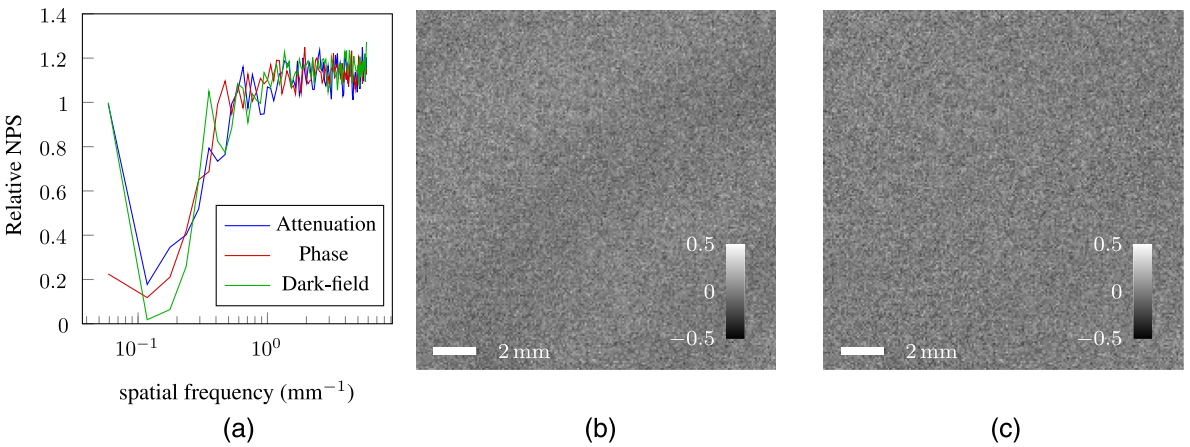

Fig. 8 Detailed results of the phase-stepping alignment for the data set where the proposed method increased the standard deviation in the homogenous region. (a) Radial NPS of the proposed method, divided by NPS of the standard reconstruction. The low-frequency NPS is decreased by an order of magnitude. The high-frequency NPS is slightly increased. (b) Differential phase reconstructed with standard method. Parts of a moiré pattern are visible. (c) Same image reconstructed with proposed stepping realignment. The moiré pattern has been removed, while the increase in high-frequency noise is hardly visible.

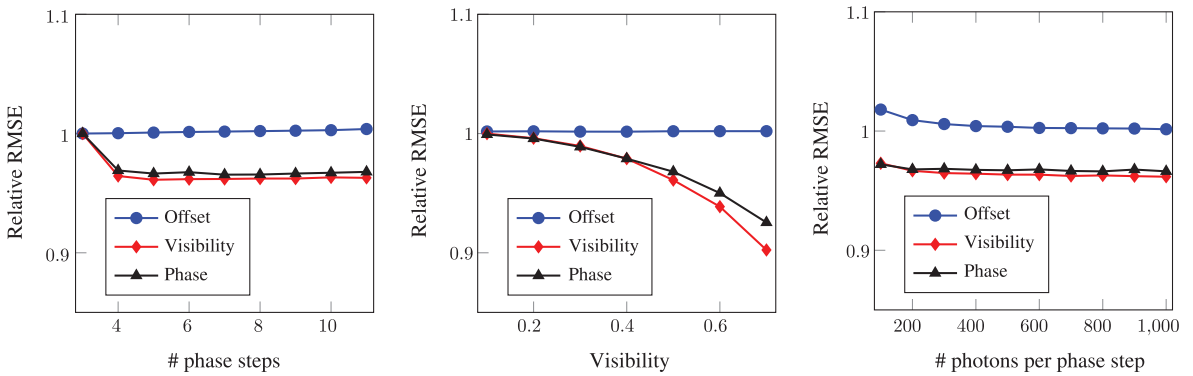

Fig. 9 Reconstruction results for noise variance weighting evaluation on simulated data. The plots show the RMSE to ground truth obtained with the proposed weighting, divided by the RMSE obtained with the standard method. Error bars were negligible and omitted for clarity. We vary the number of phase steps, the visibility, and the mean photon count per phase step while we keep the other parameters constant. The benefit of the proposed noise weighting increases with a higher visibility. For a low number of photons, the proposed method slightly increases the offset error. This is because our Gaussian approximation of the Poisson noise distribution is only valid for a sufficiently high number of photons.

the offset information does not benefit from noise weighting. The benefit for these two images shows a strong nonlinear dependency on the visibility. A relatively high visibility of at least 60% is required for a noise reduction exceeding 5% in visibility and phase. For low photon counts below about 200, the actual error with noise weighting increases for the offset information. We attribute this to the fact that we approximate a Poisson distribution with a Gaussian distribution, which may lead to errors at low photons counts.

To verify our simulation results, we computed the relative standard deviation in a homogeneous region of a sample data set in a similar fashion as for the experiment assessing the phase-stepping position correction. Here, we obtained a reduction in standard deviation of 0.0% for attenuation, 0.6% for the dark-field image, and 0.4% for the differential phase. These numbers are in line with our simulation results, which predicted 0.0% for the offset, 0.5% for visibility, and 0.5% for the phase at the low mean free-field visibility of 23% of this data set.

3.3.1 *Discussion*

The experiments have shown that noise variance weighting in phase-stepping reconstruction reduces phase and visibility noise if the visibility is high and if a sufficient number of photons contribute to the measurements. It has recently been demonstrated[40] that visibilities exceeding 50% can be achieved using conventional x-ray sources. In this context, the noise variance weighting is an improvement that is straightforward to implement, can improve image quality, and only slightly increases computational demand. For data with a very low number of photons, we obtained a slight increase in error for the offset information. This can be avoided by switching between weighted and unweighted reconstruction of offset data based on the recorded intensity. For future work, it may be worthwhile to investigate the use of other data likelihood functions known from iterative absorption CT reconstruction.

3.4 *Visibility Bias Correction*

We used Monte Carlo simulation to assess the proposed visibility bias correction. To this end, we again generated phase-stepping data affected by quantum noise. Afterward, we reconstructed offset, visibility, and phase using the standard method and using the proposed visibility bias correction. We generate 100,000 noise realizations and compared the resulting mean and standard deviation of the reconstructed visibility to the ground truth visibility. Our baseline scenario is low-SNR acquisition with an offset corresponding to 100 photons, a visibility of 0.2, a random phase, and three phase steps. In the first experiment, we vary the visibility while in the second experiment, we vary the photon counts.

The results of the experiments are shown in Fig. 10. The results show that the standard method overestimates the visibility, where the degree of the overestimation increases with decreasing visibility and photon number. The proposed method shows no substantial overestimation for the baseline scenario, but only a slight overestimation when visibility or photon count is decreased even further. Visibilities reconstructed with bias correction have standard deviations that are 5% to 20% higher than the deviations obtained without the correction. The increase in standard deviations is proportional to the reduction in estimation bias.

We also applied the visibility correction to two data sets acquired with a Talbot–Lau interferometer. The first data set is one of the breast data sets. Here, it can be observed that the correction leads to an increased dark-field signal at strongly absorbing metal inserts used to fixate the specimen [see Fig. 10(c)]. This can be attributed to the correction of an overestimation of the object visibility at this point, which leads to an increased dark-field signal. We also acquired dark-field images of a foam wedge [length: 11.9 cm, width: 2.8 cm, thickness: increasing from 0 to 6.1 cm, shown in Fig. 10(d)]. Images were acquired with a low-dose protocol (0.25 mAs) and a high-dose protocol (15 mAs). Four phase steps were acquired for both protocols. The foam wedge was placed on a PMMA plate such that the thickness linearly increases from the left to the right. The resulting dark-field images are averaged over the width of the wedge to yield a plot of the dark-field signal over the wedge thickness. We plot the results obtained for the high- and the low-dose protocol, both with the standard and the proposed reconstruction in Fig. 10(e). The dark-field value of the low-dose image reconstructed with the standard method is underestimated with increasing dark field (or decreasing object visibility, respectively). The proposed method reduces

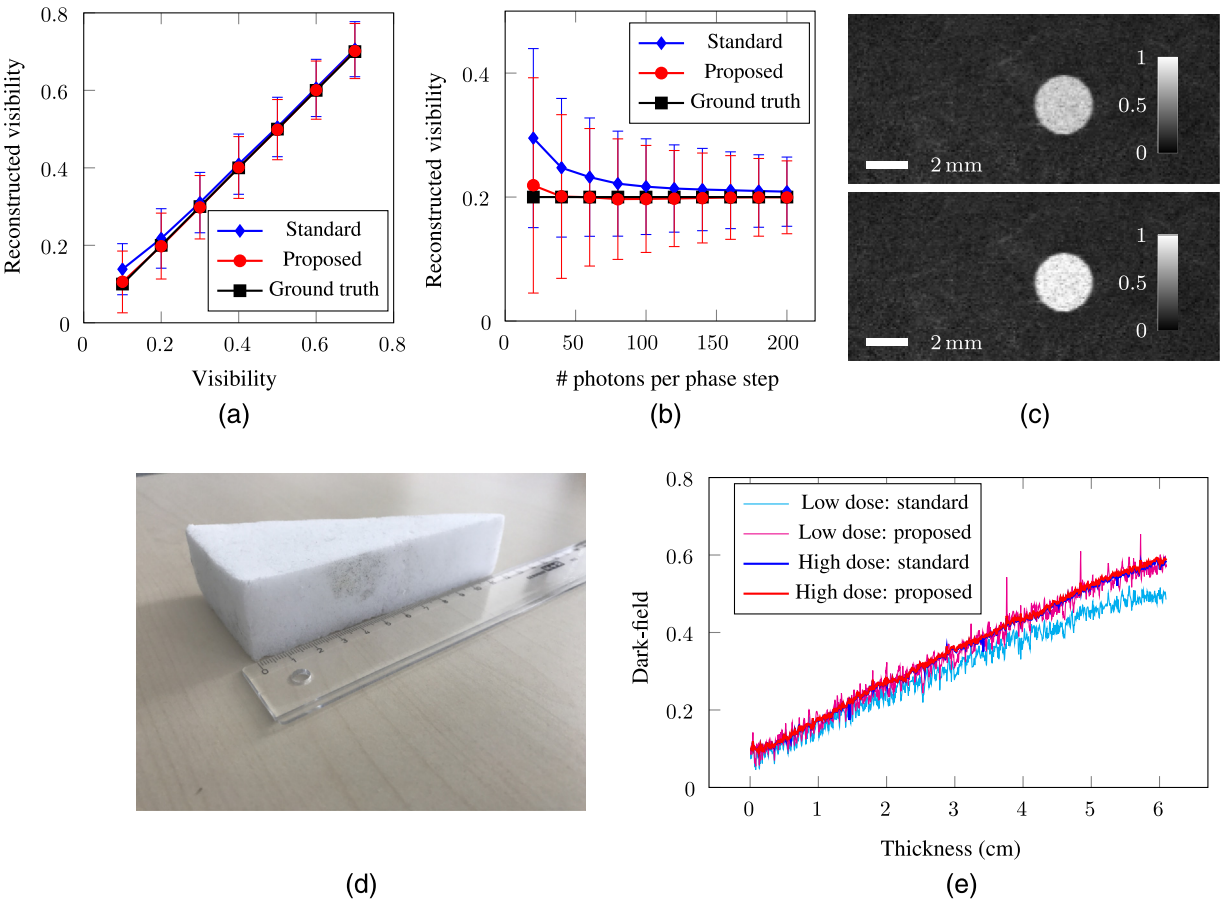

Fig. 10 Evaluation of the visibility bias correction. (a and b) Results of visibility reconstruction from simulated phase-stepping data using Monte Carlo simulation. The baseline scenario is a low-SNR acquisition with three phase steps, 100 photons per phase step, and a visibility of 0.2. In the left figure, we vary the visibility. In the right figure, we vary the average number of photons per phase step. The standard method overestimates the visibility when the photon counts or the visibility is low. The proposed method reduces the estimation bias and is closer to the ground truth, at the cost of a slightly increased standard deviation. (c) Dark-field image of metal insert embedded in a human breast specimen reconstructed without (top) and with (bottom) visibility bias correction. (d) Photograph of foam wedge. (e) Plot of the reconstructed dark-field signal of the foam wedge. Sample thickness increases linearly along the *x*-axis. The *y*-axis shows the reconstructed dark-field signal for a low- and a high-dose scan using standard reconstruction and the proposed bias correction.

this bias, which can be seen from the overlapping curves of the proposed correction on the low-dose scan and the uncorrected high-dose scan. This behavior is also in accordance with the simulations.

3.4.1 *Discussion*

The experiments confirm the findings by Marschner et al.[22] of an estimation bias in the visibility. Our proposed bias correction method effectively reduced the estimation bias and even yields an unbiased estimate up to a very low SNR. The use of the bias correction might be particularly useful for lung imaging, which has emerged as a possible application for dark-field imaging.[15,16] A drawback of the bias correction is an increase in the standard deviation of the reconstructed visibility, i.e., in image noise. This is due to the fact that the offset (which itself is affected by noise) is used to correct for the bias. However, increased noise can be tackled by spatial denoising of either the reconstructed visibilities or the offsets used for the correction. This is not possible for the estimation bias, since it is a systematic error. For future work, it may be worthwhile to study other methods for magnitude bias reduction that have been developed by the MR imaging community.

4 Conclusions

Phase-stepping reconstruction is a key step in Talbot–Lau imaging. In this paper, we reviewed the underlying assumptions that are used in phase-stepping reconstruction. We find that some of these assumptions, namely known phase-stepping positions, equal noise variance in all phase steps and no systematic estimation error, may be violated under certain conditions. We proposed an optimization-based method to estimate phase-stepping positions affected by interferometer misalignment. Our evaluation on real and simulated data has shown that our method can reduce or even remove moiré artifacts, which arise from misaligned phase-stepping positions. We furthermore proposed a weighting function to account for differences in noise variance of the phase-stepping data. Our evaluation has shown that the proposed changes may lead to a meaningful noise reduction

for high-visibility acquisitions when the number of photons per phase step is sufficiently high. We verified previous observations that phase-stepping reconstruction overestimates the visibility when the visibility SNR is low. A correction strategy for reducing this estimation bias has been proposed and evaluated on simulated data. It has been shown that the proposed strategy can compensate the overestimation up to a lower bound on visibility and photon counts, at the expense of slightly increased noise. Since the methods are independent of each other, they can readily be integrated into an existing framework for phase-stepping reconstruction. We expect that these methods will improve image quality in Talbot–Lau imaging.

Disclosures

The authors have no relevant financial interests in the paper and no other potential conflicts of interest to disclose.

Acknowledgments

Sebastian Kaeppler gratefully acknowledges funding from the International Max Planck Research School—Physics of Light. This work was partially supported by the Research Training Group 1773 Heterogeneous Image Systems funded by the German Research Foundation (Deutsche Forschungsgemeinschaft). We would like to thank the anonymous reviewers for their valuable feedback.

References

1. S. W. Wilkins et al., "Phase-contrast imaging using polychromatic hard x-rays," *Nature* **384**, 335–338 (1996).
2. C. Parham et al., "Design and implementation of a compact low-dose diffraction enhanced medical imaging system," *Acad. Radiol.* **16**, 911–917 (2009).
3. P. R. Munro et al., "Phase and absorption retrieval using incoherent x-ray sources," *Proc. Natl. Acad. Sci. U. S. A.* **109**(35), 13922–13927 (2012).
4. A. Momose et al., "Demonstration of x-ray Talbot interferometry," *Jpn. J. Appl. Phys.* **42**, L866–L868 (2003).
5. F. Pfeiffer et al., "Phase retrieval and differential phase-contrast imaging with low-brilliance x-ray sources," *Nat. Phys.* **2**, 258–261 (2006).
6. M. Bech et al., "Soft-tissue phase-contrast tomography with an x-ray tube source," *Phys. Med. Biol.* **54**, 2747–2753 (2009).
7. T. Donath et al., "Toward clinical x-ray phase-contrast CT: demonstration of enhanced soft-tissue contrast in human specimen," *Invest. Radiol.* **45**, 445–452 (2010).
8. A. Tapfer et al., "Experimental results from a preclinical x-ray phase-contrast ct scanner," *Proc. Natl. Acad. Sci. U. S. A.* **109**(39), 15691–15696 (2012).
9. F. Pfeiffer et al., "Hard-x-ray dark-field imaging using a grating interferometer," *Nat. Mater.* **7**, 134–137 (2008).
10. S. K. Lynch et al., "Interpretation of dark-field contrast and particle-size selectivity in grating interferometers," *Appl. Opt.* **50**, 4310–4319 (2011).
11. M. Bech et al., "In-vivo dark-field and phase-contrast x-ray imaging," *Sci. Rep.* **3**, 3209 (2013).
12. F. L. Bayer et al., "Reconstruction of scalar and vectorial components in x-ray dark-field tomography," *Proc. Natl. Acad. Sci. U. S. A.* **111**, 12699–12704 (2014).
13. M. Stampanoni et al., "The first analysis and clinical evaluation of native breast tissue using differential phase-contrast mammography," *Invest. Radiol.* **46**(12), 801–806 (2011).
14. S. Grandl et al., "Improved visualization of breast cancer features in multifocal carcinoma using phase-contrast and dark-field mammography: an ex vivo study," *Eur. Radiol.* **25**(12), 3659–3668 (2015).
15. A. Yaroshenko et al., "Pulmonary emphysema diagnosis with a preclinical small-animal x-ray dark-field scatter-contrast scanner," *Radiology* **269**, 427–433 (2013).
16. K. Hellbach et al., "In vivo dark-field radiography for early diagnosis and staging of pulmonary emphysema," *Invest. Radiol.* **50**(7), 430–435 (2015).
17. A. Momose et al., "X-ray phase imaging: from synchrotron to hospital," *Philos. Trans. R. Soc. A: Math. Phys. Eng. Sci.* **372**(2010), 20130023 (2014).
18. E. Roessl et al., "Clinical boundary conditions for grating-based differential phase-contrast mammography," *Philos. Trans. R. Soc. A: Math. Phys. Eng. Sci.* **372**(2010), 20130033 (2014).
19. T. Weitkamp et al., "Tomography with grating interferometers at low-brilliance sources," *Proc. SPIE* **6318**, 63180S (2006).
20. N. Bevins et al., "Multicontrast x-ray computed tomography imaging using Talbot–Lau interferometry without phase stepping," *Med. Phys.* **39**(1), 424–428 (2012).
21. C. Arboleda, Z. Wang, and M. Stampanoni, "Tilted-grating approach for scanning-mode x-ray phase contrast imaging," *Opt. Express* **22**(13), 15447–15458 (2014).
22. M. Marschner et al., "Two-shot x-ray dark-field imaging," *Opt. Express* **24**(23), 27032–27045 (2016).
23. P. Modregger et al., "Imaging the ultrasmall-angle x-ray scattering distribution with grating interferometry," *Phys. Rev. Lett.* **108**(4), 048101 (2012).
24. T. Weber et al., "Increasing the darkfield contrast-to-noise ratio using a deconvolution-based information retrieval algorithm in x-ray grating-based phase-contrast imaging," *Opt. Express* **21**(15), 18011–18020 (2013).
25. Y. Yang et al., "Grating-based x-ray differential phase contrast imaging with twin peaks in phase-stepping curves—phase retrieval and dewrapping," *Med. Phys.* **43**(6), 2855–2869 (2016).
26. G. Pelzer et al., "Reconstruction method for grating-based x-ray phase-contrast images without knowledge of the grating positions," *J. Instrum.* **10**(12), P12017 (2015).
27. M. Seifert et al., "Optimisation of image reconstruction for phase-contrast x-ray Talbot–Lau imaging with regard to mechanical robustness," *Phys. Med. Biol.* **61**(17), 6441–6464 (2016).
28. J. Vargas, J. A. Quiroga, and T. Belenguer, "Phase-shifting interferometry based on principal component analysis," *Opt. Lett.* **36**(8), 1326–1328 (2011).
29. M. Marschner et al., "Helical x-ray phase-contrast computed tomography without phase stepping," *Sci. Rep.* **6**, 23953 (2016).
30. D. Hahn et al., "Statistical iterative reconstruction algorithm for x-ray phase-contrast CT," *Sci. Rep.* **5**, 10452 (2015).
31. D. Pelliccia et al., "A three-image algorithm for hard x-ray grating interferometry," *Opt. Express* **21**(16), 19401–19411 (2013).
32. P. J. Rousseeuw and A. M. Leroy, *Robust Regression and Outlier Detection*, John Wiley & Sons, Hoboken, New Jersey (2005).
33. R. Fletcher, *Practical Methods of Optimization*, John Wiley & Sons, Hoboken, New Jersey (1987).
34. H. Gudbjartsson and S. Patz, "The Rician distribution of noisy MRI data," *Magn. Reson. Med.* **34**(6), 910–914 (1995).
35. T. Weber et al., "Noise in x-ray grating-based phase-contrast imaging," *Med. Phys.* **38**, 4133–4140 (2011).
36. T. Michel et al., "On a dark-field signal generated by micrometer-sized calcifications in phase-contrast mammography," *Phys. Med. Biol.* **58**, 2713–2732 (2013).
37. S. Kaeppler et al., "Talbot–Lau x-ray phase contrast for tiling-based acquisitions without reference scanning," *Med. Phys.* **44**(5), 1886–1898 (2017).
38. W. Segars et al., "4D XCAT phantom for multimodality imaging research," *Med. Phys.* **37**(9), 4902–4915 (2010).
39. A. Maier et al., "CONRAD—a software framework for cone-beam imaging in radiology," *Med. Phys.* **40**(11), 111914 (2013).
40. J. Rieger et al., "Designing the phase grating for Talbot–Lau phase-contrast imaging systems: a simulation and experiment study," *Opt. Express* **24**(12), 13357–13364 (2016).

Sebastian Kaeppler is a PhD student at the Pattern Recognition Lab, University of Erlangen-Nuremberg. He received his BS and MS degrees in computer science from the University of Erlangen-Nuremberg in 2011 and 2014, respectively. His current research interests include x-ray imaging, signal processing, machine learning, and mathematical optimization.

Biographies for the other authors are not available.